ARTICLE IN PRESS

Optics Communications ▮ (▮▮▮▮) ▮▮▮–▮▮▮

Contents lists available at ScienceDirect

Optics Communications

journal homepage: www.elsevier.com/locate/optcom

# Simultaneous multiplane imaging with programmable multiplexed gratings

Chen Yen Lin [a,b], Yuan Luo [b,c,*]

[a] Department of Electrical Engineering and Graduate Institute of Photonics and Optoelectronics, National Taiwan University, Taipei 10617, Taiwan, ROC
[b] Institute of Medical Device and Imaging, National Taiwan University, Taipei, 10051, Taiwan, ROC
[c] Molecular Imaging Center, National Taiwan University, Taipei 10055, Taiwan, ROC

ARTICLE INFO

*Keywords:*
Optical microscopy
Three-dimensions imaging
Spatial light modulator

ABSTRACT

Microscopy has been widely used to obtain three-dimensional images of a biological sample. However, it requires a scanning in axial direction and considerable time to acquire multiple depths information of a volumetric sample. In this paper, we demonstrate a method for single-shot multi-plane imaging based on programmable multiplexed grating patterns with no mechanical moving parts by using a digital micro-mirror device (DMD). The multiplexed grating pattern displayed on DMD, in a Fourier plane, splits light into separated beam paths and are able to compensate aberrations from the proposed system. In addition, resolution can be improved using an aberration-corrected multiplexed gratings pattern. We present and characterize the design, implementation, and experimentally demonstrate the proposed system's ability through simultaneous multiple planes imaging of the biological samples.

## 1. Introduction

Conventional wide field microscopy requires scanning to sequentially acquire two-dimensional (2D) images of a biological sample to form a three-dimensional (3D) stack. However, scanning in depth is a relatively slow approach to observe an instant biological event, and mechanical moving parts may also disturb a living sample during imaging. Instead of mechanical scanning, a focus tunable lens including a membrane and optical grade fluid in a Fourier plane has been utilized to control a focal length of a microscope to electronically scan a volumetric sample [1]. There exists a wealth of alternatives to reduce mechanical scanning, and some recent examples are remote focusing and digital refocusing. Remote focusing applies three microscopic systems to achieve axial scanning without introducing the spherical aberration [2], while digital refocusing replaces conventional light sources by a LED array [3]. Each LED is turned on and off to illuminate a sample with an oblique angle, and each 2D image at different axial planes is computed through recorded images.

To reduce or eliminate scanning, diffractive optical elements (DOEs) [4–6] have been applied to form a multi-focus system for one-shot 3D imaging acquisition since DOE diffracts light from different depths within a sample with specific traveling directions and displays depths onto different portions of an image plane. The most recent methods include quadratically distorted (QD) gratings, multifocus grating (MFG) and volume holographic gratings (VHGs) [4–6].

In the former, although QD gratings and MFG, formed in a thin material, it simultaneously acquires multi-depth images of a sample, without the need of multiplexing techniques during recording process. In the latter, DOEs superimposed in a volumetric recording material provide high multiplexing capability such that each grating obtains depth-resolved information from multiple depths within the object. QD gratings, MFG and VHGs are not programmable and still need additional axial scanning to obtain images between depths. Recently, liquid crystal based spatial light modulators (LC-SLMs) have been utilized to eliminate mechanical moving parts in microscopy [7,8]. Although LC-SLM is an efficient way to display a DOE pattern, it is polarization sensitive and requires a phase calibration data [9,10].

Here, we experimentally demonstrate a mechanical-scan-free, high-resolution microscope for 3D volumetric imaging of biological samples, where the imaging speed are achieved from a combination of digital micro-mirror device (DMD) and a multiplexed grating pattern with constant magnification formation for bright-field imaging as well as dark field applications. Unlike LC-SLM based microscopy, our approach achieves high-speed operation and do not require an algorithm to obtain an optimal phase [11]. The operation speed of DMD device is faster than LC-SLMs. Therefore, our approach does not rely on mechanical moving parts to realize a *real-time* 3D imaging.

* Correspondence to: Institute of Medical Device and Imaging, College of Medicine, National Taiwan University, No. 1, Sec. 1, Jen Ai Rd., Zhongzheng Dist., Taipei City 10051, Taiwan, ROC.
*E-mail address:* yuanluo@ntu.edu.tw (Y. Luo).

https://doi.org/10.1016/j.optcom.2018.02.059
Received 1 August 2017; Received in revised form 30 December 2017; Accepted 24 February 2018
Available online xxxx


Please cite this article in press as: C.Y. Lin, Y. Luo, Simultaneous multiplane imaging with programmable multiplexed gratings, Optics Communications (2018), https://doi.org/10.1016/j.optcom.2018.02.059.

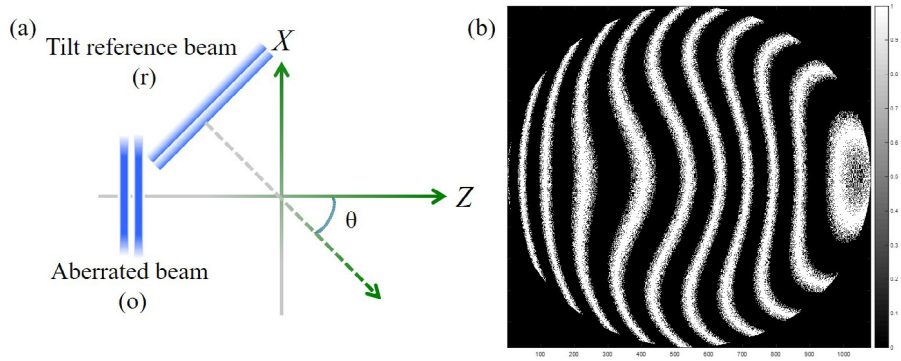


**Fig. 1.** Schematic of two beam interference. (a) The tilted beam ($r$) with a flat wavefront is incident at the observation plane at an angle, $\theta$ and an aberrated beam denoted as o travels along $z$-axis. (b) The binary interferogram results from two beam interference as beam $o$ contains aberrations ($W_{020} = +3.9\lambda$, $W_{040} = -3.8\lambda$ and $d = 0.4$ mm).

## 2. Basic principle of multi-focus multiplexed gratings

A grating pattern displayed on DMD can be interpreted as an interferogram [12], which is commonly observed in a two-beam Mach–Zehnder interferometer. Assuming two beams in the form of a planar wavefront, the period of straight line fringes is described as $d = \lambda/\sin\theta$, where $\lambda$ is wavelength of light. The incident angle, $\theta$, determines the spatial frequency of fringes on the observation plane, $x$ in Fig. 1.

In Fig. 1, a tilted beam with a planar wavefront is denoted as $r$ and the object beam with an aberrated wavefront is denoted as $W_o$. The varied optical properties of these two beams lead to the various kinds of interferograms as shown in Fig. 1(b).

Since the inference grating pattern can be displayed onto DMD, the intensity distribution of the pattern on the DMD can be written as

$$I(x,y) = 0.5\left(1 + \cos\left[k\left(W_r + W_o\right)\right]\right), \tag{1}$$

where $k = 2\pi/\lambda$ and $W_r$ is equal to $x\sin(\theta)$ in Fig. 1. The object beam with an aberrated wavefront includes all the wavefront coefficients in term of Seidel aberrations. The function of the $W_o$ is intended to include a defocus wavefront and compensate other aberrations existing in the system. A similar approach to reduce the spherical aberration in digital holography has been discussed by Alexander et al. in 2000 [13].

For an on-axis object point at a defocus position away from the nominal focal plane, only spherical aberration is dominated inside an optical system. The acceptance angle of the objective lens is determined by the numerical aperture (NA). In order to correct the depth induced spherical aberration, the Abbe sine condition is taken into consideration into the pattern design. To satisfy Abbe sine condition, the relationship between the paraxial acceptance angle denoted as $\theta_{in}$ and the real acceptance angle denoted as $\alpha$ has to be linear. Namely $\rho = \sin\theta_{in}/\sin\alpha = r_{ap}/R$, where $r_{ap}$ and $R$ is the radial coordinate of the aperture and the radius of the aperture, respectively. The optical path difference (OPD) between a spherical reference wavefront [14] and an aberrated wavefront, $W_o$, is expressed as

$$W_o = \delta z\left[1 - \sqrt{1 - \left(\frac{r_{ap}}{f_{relay2}}\right)^2}\right] + \sum_{klm} W_{klm} h^k \rho^l \cos^m(\theta) \tag{2}$$

where $\delta z$ is a defocus distance setting up the spacing between a nominal focal plane and defocus plane, $f_{relay2}$ is the focal length of a relay lens in Fig. 2 and $W_{klm}$ represents the Seidel aberrations, including a spherical aberration, $W_{040}\rho^4$, etc.

As one point source is shifted away from the front focal point of second relay lens in $\delta z$, the corresponding defocus wavefront is the first term of Eq. (2). Without considering defocus $OPD$ in the paraxial approximation, the relationship between the $\delta z$ in the intermediate image space and the defocus $OPD(= W_{020})$, is written as

$$OPD_{defocus} = \delta z\left[1 - \sqrt{1 - \left(\frac{r_{ap}}{f_{relay2}}\right)^2}\right] \tag{3}$$

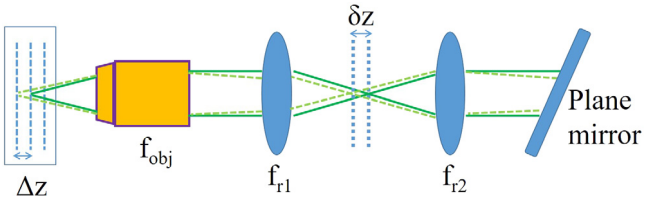


**Fig. 2.** The setup of the object lens ($f_{obj}$) and two relay lenses ($f_{r1}$ and $f_{r2}$). The focal plane spacing $\Delta z$ determines the depth separation of each image plane. The defocus distance, $\delta z$, in the intermediate image space have a relationship with $\Delta z$ described by Eq. (4).

where $f_{relay2}$ (=$f_{r2}$ in Fig. 2). As Eq. (3) is taken in the first order of Taylor expansion approximation, it can be rewritten as $\delta z = 2(f_{r2}/r_{ap})^2 OPD_{defocus}$ [4]. In Fig. 2 the $\delta z$ is the defocus distance in the intermediate image space. The focal plane spacing, $\Delta z$, in the object space is calculated as

$$\Delta z = \left(\frac{f_{obj}}{f_{relay1}}\right)^2 \delta z \tag{4}$$

where $f_{obi}$ and $f_{relay1}$ (=$f_{r1}$ in Fig. 2) is focal length of the objective lens and the first relay lens, respectively.

The multiplexed binary grating patterns can be stored in the internal memory of the DMD and saved in bmp file format for the DMD to display sequentially. The speed of the DMD operated in a binary mode can reach 9523 Hz. A multiplexed grating pattern consists of the two crossed interferograms, which are superimposed on top of each other as shown in Fig. 3(a). However, once a continuous grayscale pattern becomes a binary pattern, it results in a non-linear quantization error if only a simple threshold is applied. The Floyd–Steinberg algorithm (dithering) pushes the residual error to neighboring pixels and mimic the original grayscale pattern [15]. For example, the multiplexed binary grating pattern is shown in Fig. 3(a). The zoom-in image in Fig. 3(a) shows through the manipulation of the density of the white spots to mimic the sinusoidal grating pattern. The focal plane spacing along horizontal direction ($\Delta z_h$) is setting as 4 μm, while the spacing along vertical direction ($\Delta z_v$) is chosen as $3\Delta z_h$ in order to have an equal spacing between each focal plane. After taking the multiplexed grating pattern in Fig. 3(a) into a Fourier transform, the point spread function (PSF) of the grating pattern and their corresponding defocus distances are shown in Fig. 3(b) and (c), respectively.

## 3. Experimental results

The schematic diagram for a simultaneous multi-planes imaging system is shown in Fig. 4. The trans-illumination module consists of



Please cite this article in press as: C.Y. Lin, Y. Luo, Simultaneous multiplane imaging with programmable multiplexed gratings, Optics Communications (2018), https://doi.org/10.1016/j.optcom.2018.02.059.